ELSEVIER

International Journal of Solids and Structures 41 (2004) 1491–1518

INTERNATIONAL JOURNAL OF SOLIDS and STRUCTURES

www.elsevier.com/locate/ijsolstr

A new super convergent thin walled composite beam element for analysis of box beam structures

Mira Mitra, S. Gopalakrishnan *, M. Seetharama Bhat

Department of Aerospace Engineering, Indian Institute of Science, C.V. Raman Road, Bangalore 560012, India

Received 9 April 2003; received in revised form 15 October 2003

Abstract

In this paper, a new composite thin wall beam element of arbitrary cross-section with open or closed contour is developed. The formulation incorporates the effect of elastic coupling, restrained warping, transverse shear deformation associated with thin walled composite structures. A first order shear deformation theory is considered with the beam deformation expressed in terms of axial, spanwise and chordwise bending, corresponding shears and twist. The formulated locking free element uses higher order interpolating polynomial obtained by solving static part of the coupled governing differential equations. The formulated element has super convergent properties as it gives the exact elemental stiffness matrix. Static and free vibration analyses are performed for various beam configuration and compared with experimental and numerical results available in current literature. Good correlation is observed in all cases with extremely small system size. The formulated element is used to study the wave propagation behavior in box beams subjected to high frequency loading such as impact. Simultaneous existence of various propagating modes are graphically captured. Here the effect of transverse shear on wave propagation characteristics in axial and transverse directions are investigated for different ply layup sequences.

Keywords: Thin walled beam; Finite element; Free vibration; Wave propagation

1. Introduction

Composites are being used widely as construction material in aircraft industries because of their high strength to weight ratio, increased fatigue life and improved damage tolerant nature. Thin walled structures are integral parts of an aircraft. In many structures like rotor blades, wing spars etc they can be modeled as one dimensional beam as the sectional dimensions are much small compared to the length. Several non-classical behavior are exhibited by thin walled composite structures which includes the effect of elastic coupling, transverse shear deformation and restrained torsional warping. These characteristics can be exploited to improve efficiency through proper modeling.

* Corresponding author. Tel.: +91-80-2933019; fax: +91-803600134.
E-mail addresses: mira@aero.iisc.ernet.in (M. Mitra), krishnan@aero.iisc.ernet.in (S. Gopalakrishnan), msbdcl@aero.iisc.ernet.in (M. Seetharama Bhat).

0020-7683/$ - see front matter © 2003 Elsevier Ltd. All rights reserved.
doi:10.1016/j.ijsolstr.2003.10.024

The influence of transverse shear deformation cannot be neglected even in comparatively slender composite beams because of low shear modulus to direct modulus ratio (Davalos et al., 1994; Kant and Gupta, 1988). The effects are more significant for high frequency responses, where Euler Bernoulli beam theory (EBT) gives exorbitantly high wave speeds. In thin walled composite beam, the end restrains causes non uniform out-of-plane torsional warping as opposed to Saint Venant's assumptions. This effect is predominant in open section beam and in such cases Vlasov theory is normally adopted to incorporate restrained warping effect, which causes considerable change in the effective torsional stiffness.

The box beam is normally analyzed using a 1-D mathematical model, but representing 3-D motion. 1-D approximations are associated with assumption of local displacements in terms of generalized beam displacements namely extension, bending in two directions, shear in two directions and twist. A survey of existing numerical and analytical thin walled composite beam theories was done by Jung et al. (1999a,b) and Volovoi et al. (2001). A variational-asymptotic approach has been adopted by several researchers for the above modeling problem. It helps in an efficient reduction of 3-D elasticity problem to 1-D beam problem. Analytical cross-sectional models based on variational- asymptotic formulation were presented by Berdichevsky et al. (1992), Badir et al. (1993) and Volovoi and Hodges (2002). Apart from the analytical modeling of the beam cross-section, asymptotically correct finite element modeling techniques has also been developed. VABS (Variational Asymptotic Beam Section Analysis) was developed by Cesnik and Hodges (1997) which derive the cross-sectional stiffness through finite element discretization. A finite element based cross-sectional analysis using variational asymptotic method and incorporating transverse shear effect is presented by Popescu and Hodges (1999). A first order shear deformable analytical cross-sectional modeling technique was proposed by Jung et al. (2002) without neglecting in-plane bending moments.

In first order shear deformation theory (FSDT) and higher order shear deformation theories (HSDT), finite element formulation requires C^o continuous elements for independent interpolation of transverse displacement and slope. Shear constraints are always associated with these C^o elements. When thin beams are discretized using such elements, they do not yield zero shear strains. This is defined as the shear locking problem. A shear locked element causes considerable under estimation of deformation. With the above inconsistent formulation, the problem of shear locking can be eliminated using selective or reduced integration (Averill and Reddy, 1990).

All constraint media problems, like shear locking problem leads to two sets of stiffness matrix. One from unconstrained strain field and the other from the constrained strain field. For shear deformable elements, the bending stiffness matrix $[K_B]$ comes from the unconstrained strain field, while the shear stiffness matrix $[K_S]$ comes from the constrained strain field. Matrix $[K_S]$ is also called the Penalty matrix. The problem is thus reduced to solving the matrix equation

$$[[K_B] + \alpha[K_S]]\{u\} = \{f\} \tag{1}$$

where $\{u\}$ and $\{f\}$ are the nodal displacements and forces and α is the penalty parameter. In the penalty limit as the beam becomes thin, α value becomes very large and for accurate solution, $[K_S]$ requires to be singular. One way of eliminating the problem is to perform reduced integration on the penalty matrix $[K_S]$ to make it rank deficient. This ensures that $[K_S]$ is singular and proper solutions can be obtained. Hence, numerical integration plays a crucial role in getting proper solutions in the constrained media problems.

Consistent finite element can be alternatively formulated using interpolating polynomials that are exact solutions to the governing equations. This approach was implemented to obtain shape functions for an isotropic three-dimensional Timoshenko beam (Bazoune et al., 2003) and in deriving exact stiffness matrix in higher order isotropic beam (Eisenberger, 2003), in FSDT asymmetric composite beams (Chakraborty et al., 2001), for higher order isotropic rod (Gopalakrishnan, 2000), for first order shear deformable isotropic beams (Friedman and Kosmatka, 1993), for first and higher order shear deformable isotropic beams (Khedir and Reddy, 1997; Reddy, 1997). In these elements, some constants of the interpolating polynomials are dependent on material and cross-sectional properties. Here, the degrees of interpolation functions

depends on the orders of governing equations and as the beam becomes thin, all these material dependent constants transform themselves in such a manner that elementary solutions are recovered. The advantage is that the user need not know whether the shear deformation is significant. With similar physical implication, interpolation functions in terms of series were used in (Eisenberger, 1994) that reduced to continuum solution when higher number terms were considered in the solution. In this paper, this approach is adopted to derive the exact stiffness matrix of a thin walled composite beam.

In the present paper a generic composite thin walled beam element having arbitrary cross-section with open and closed contour is developed. The element uses higher order interpolating polynomials that are derived by solving the static homogeneous coupled governing differential equation and hence predicts the exact elemental stiffness matrix. Each node has 6 degrees of freedom including extension, two in bending in spanwise and chordwise directions, corresponding shears and twist. First order theory is used for transverse shear deformation and out-of-plane torsional warping is modeled using Vlasov theory. Higher order interpolating polynomial for twist eliminates the need of separate degree of freedom for restrained torsional warping resulting in 6×6 elemental stiffness matrix compared to 7×7 stiffness matrix required by conventional finite element.

The dynamic analysis of thin walled composite beams are generally performed by extending the cross-sectional models, particularly to study the effect of various cross-sectional parameters, ply layup sequences on the free vibration responses. Free vibration analyses of composite beams was done by Hodges et al. (1991) and Song and Librescu (1997) for non rotating and closed cross-section rotating beams respectively. They studied the influence of ply orientation and elastic couplings on natural frequencies. Jung et al. (2001) performed dynamic analyses of rotating and non rotating beam from an analytical cross-sectional model proposed by Jung et al. (1999a,b). Effect of wall thickness and transverse shear on natural frequencies was discussed.

The modeling approach can be briefly outlined as (1) local displacements are obtained from generalized beam displacements, which are functions of spanwise coordinate x and time t; (2) plane stress assumption is used to derive the constitutive relation; (3) strain and kinetic energies are evaluated in terms of beam displacements; (4) Hamilton's principle is used to derive the governing differential equations; (5) The static homogeneous differential equations are solved to obtain higher order shape functions; (6) the derived shape functions results in exact elemental stiffness matrix and an approximate consistent mass matrix. The formulated element is used to study the static and free vibration behavior of various flat and box beam configurations. The beams used for numerical experiments has varied material and geometric properties exhibiting different elastic coupling.

Composite beam structures subjected to high velocity impact load vibrates at higher modes that includes various local 3-D modes, apart from the beam modes. Very few literature are available in this area though such structures may be very often subjected to highly transient loading such as tool drop and other kind of impact. These relates to wave propagation problems and can be differentiated from conventional dynamic response problem by the (1) high frequency content of loading history and (2) phase transformation during propagation. The dynamics of higher order beam structures subjected to high frequency loading or impact introduces certain effect which are absent in their elementary counterparts. These effects may produce new propagating modes. Finite element formulation for wave propagation problems require large system size to capture all the higher modes as the load has a high frequency content. Hence the element size has to be comparable to wavelengths, which are very small at high frequencies. These problems are usually solved in the frequency domain and one such method is the spectral element method (SEM). SEM has been used for wave propagation problem in isotropic Timoshenko beam (Gopalakrishnan et al., 1992) and in composite Euler–Bernoulli beam (Mahapatra et al., 2000). Essential features of beam transient dynamics can be more easily captured using SEM. However, spectral element formulation, which is based on exact solutions of the governing wave equations in the transformed frequency domain, is available only for few structural elements like rods, beams, cylinders etc. As stated earlier, impact loads with high frequency content excites

many local 3-D modes, even in beam like structures. Thus the dynamic model of the beam should be capable of capturing these 3-D modes. Use of 3-D finite element for such problem is not computationally viable. Efficient cross-sectional models e.g. VABS can produce accuracy comparable to 3-D finite element (Yu et al., 2002). Such cross-sectional stiffness model can be used in beam analysis that can decrease the system size considerably. Though the present element formulation is not capable of capturing the 3-D effects, wave propagation analysis are performed to get an insight into the high frequency response of composite thin walled structures and effects of various design parameters on it. In this paper, wave propagation characteristics in longitudinal and transverse directions are studied for box beams with different ply orientation and is compared with EBT neglecting the effect of transverse shear. One of the fundamental feature associated with the mechanics of the symmetric/antisymmetric box beam is the existence of axial-shear/axial-torsion coupling in axial response and bending-torsion/ bending-shear coupling in flexural response. These are graphically captured using a high frequency modulated pulse.

This paper is organized as follows. First the governing equations for a thin walled beam of arbitrary cross-section is derived using Hamilton's principle. The finite element formulation is given next followed by numerical experiments involving static, free vibration and wave propagation analysis. The numerical results are compared with the results available in the existing literature. The paper ends with some important conclusions and future scope of further studies in making faster and cost effective finite element analysis.

2. Governing differential equation for a thin-walled beam

From the geometrical consideration and assuming in-plane deformation to be negligible, the beam displacement field can be written as

$$w = v_o z_{,s} - w_o y_{,s} - q\psi \tag{2}$$

$$v = v_o y_{,s} + w_o z_{,s} + r\psi \tag{3}$$

$$u = u_o + z\theta_y + y\theta_z - \varphi\psi_{,x} \tag{4}$$

where u_o, v_o, w_o are the displacements in x, y, z directions. ψ, θ_y, θ_z are the rotations about x, y, z directions (see Fig. 1). The torsional warping function φ is expressed as (Megson (1974))

$$\varphi = \int_0^s r\,\mathrm{d}s - 2A_c\frac{\delta_{os}}{\delta}, \quad \delta_{os} = \int_0^s \frac{\mathrm{d}s}{Gt} \quad \delta = \oint \frac{\mathrm{d}s}{Gt}$$

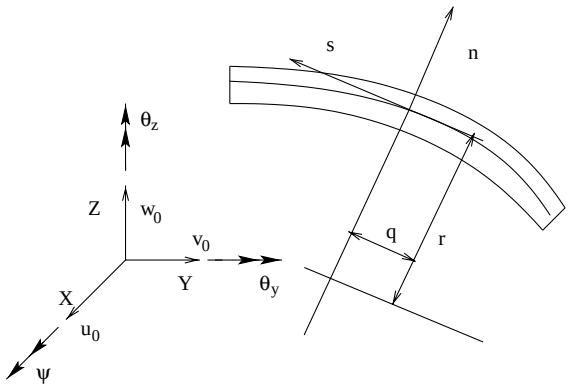

Fig. 1. Coordinate system and generalized beam displacements.

for closed cross-section, where t is the wall thickness, A_c is the cross-sectional area enclosed by mid line contour, G is the shear modulus, r is the radius, s is the tangential coordinate and n is the normal co-ordinates. For open contours, neglecting secondary warping, φ is

$$\varphi = \int_0^s r\,\mathrm{d}s$$

Strain displacement relation are derived using Eqs. (2)–(4),

$$\varepsilon_{xx} = \partial u/\partial x = u_o,x + z\theta_y,x + y\theta_z,x - \varphi\psi_{,xx} \tag{5}$$

$$\gamma_{xs} = \partial u/\partial s + \partial v/\partial x = \gamma^s_{xs} + \gamma^t_{xs} = \{(w_o,x + \theta_y)z_{,s} + (\theta_z + v_o,x)y_{,s}\} + \{(r - \varphi_{,s})\psi_{,x}\} \tag{6}$$

$$\gamma_{xn} = \partial u/\partial n + \partial w/\partial x = \gamma^s_{xn} + \gamma^t_{xn} = \{(\theta_z y_{,n} - w_o, xy_{,s}) + (\theta_y z_{,n} + v_o, xz_{,s})\} - \{(q + \varphi_{,n})\psi_{,x}\} \tag{7}$$

where ε_{xx} is the normal strain and γ_{xs}, γ_{xn} are the shear strains. γ^t_{xn} can be neglected as torsional displacement do not contribute to the shear strain in transverse direction (see Megson, 1974) and hence the transverse shear γ_{xn} can be assumed to contain only γ^s_{xn} components.

In plane stress condition, the normal stress σ_{ss} and the transverse shear stress τ_{sn} are assumed zero and the constitutive model is obtained through plane stress reduction of 3-D constitutive law. Plane stress assumption correlates better with experiment than plane strain assumption (Jung et al., 1999a,b).

$$\begin{Bmatrix} \sigma_{xx} \\ \tau_{xs} \\ \tau_{xn} \end{Bmatrix} = \begin{bmatrix} \overline{Q}_{11} & \overline{Q}_{16} & 0 \\ \overline{Q}_{16} & \overline{Q}_{66} & 0 \\ 0 & 0 & \overline{Q}_{55} \end{bmatrix} \begin{Bmatrix} \epsilon_{xx} \\ \gamma_{xs} \\ \gamma_{xn} \end{Bmatrix} \tag{8}$$

The stiffness coefficients $\overline{Q}_{ij}$ are given by

$$\begin{aligned} \overline{Q}_{11} &= Q_{11} - \frac{Q^2_{12}}{Q_{22}}, \quad \overline{Q}_{16} = Q_{16} - \frac{Q_{12}Q_{26}}{Q_{22}} \\ \overline{Q}_{66} &= Q_{66} - \frac{Q^2_{26}}{Q_{22}}, \quad \overline{Q}_{55} = Q_{55} - \frac{Q^2_{45}}{Q_{44}} \end{aligned} \tag{9}$$

where Q_{ij} are the transformed stiffness coefficients (see Jones, 1975). Total strain and kinetic energies are calculated as

$$\Pi = \frac{1}{2}\int_0^L \int_A (\sigma_{xx}\epsilon_{xx} + \tau_{xs}\gamma_{xs} + \tau_{xn}\gamma_{xn})\,\mathrm{d}A\,\mathrm{d}x \tag{10}$$

$$T = \frac{1}{2}\rho \int_0^L \int_A (\dot{u}^2_o + \dot{v}^2_o + \dot{w}^2_o)\,\mathrm{d}A\,\mathrm{d}x \tag{11}$$

where $\mathrm{d}A$ is the elemental area given by $\mathrm{d}s\,\mathrm{d}n$.

Using the Hamilton's principle, the minimization of the above energy with respect to the six degree of freedom $(u_o, v_o, w_o, \psi, \theta_y, \theta_z)$ will give the six highly coupled differential equation, which are given by

$$\begin{aligned} &I_o\ddot{u}_o + I_1\ddot{\theta}_y + \underline{I}_1\ddot{\theta}_z + I_\varphi\ddot{\psi}_{,x} - A_{11}u_{o,xx} - A_{y_s16}v_{o,xx} - A_{z_s16}w_{o,xx} + A_{\varphi 11}\psi_{,xxx} - A_{\alpha 16}\psi_{,xx} - B_{11}\theta_{y,xx} \\ &\quad - A_{z_s16}\theta_{y,x} - \underline{B}_{11}\theta_{z,xx} - A_{y_s16}\theta_{z,x} \\ &\quad = 0 \end{aligned} \tag{12}$$

$$\begin{aligned} &(I_{z_s^2} + I_{y_s^2})\ddot{v}_o - (I_{z_s q} - I_{y_s r})\ddot{\psi} - A_{y_s16}u_{o,xx} - (A_{y_s^2 66} + A_{z_s^2 55})v_{o,xx} - (A_{z_s y_s 66} - A_{z_s y_s 55})w_{o,xx} + A_{y_s\varphi 16}\psi_{,xxx} \\ &\quad - A_{y_s\alpha 66}\psi_{,xx} - B_{y_s16}\theta_{y,xx} - (A_{z_s y_s 66} + A_{z_s z_n 55})\theta_{y,x} - \underline{B}_{y_s16}\theta_{z,xx} - (A_{y_s^2 66} + A_{y_n z_s 55})\theta_{z,x} \\ &\quad = 0 \end{aligned} \tag{13}$$

$$(I_{z_s^2}+I_{y_s^2})\ddot{w}_o+(I_{y_sq}+I_{z_sr})\ddot{\psi}-A_{z_s16}u_{o,xx}-(A_{y_sz_s66}-A_{y_sz_s55})v_{o,xx}-(A_{z_s^2}66+A_{y_s^2}55)w_{o,xx}+A_{z_s\varphi16}\psi_{,xxx}$$
$$-A_{z_s\alpha66}\psi_{,xx}-B_{z_s16}\theta_{y,xx}-(A_{z_s^2}66-A_{y_sz_n55})\theta_{y,x}-\underline{B}_{z_s16}\theta_{z,xx}-(A_{y_sz_s66}-A_{y_ny_s55})\theta_{z,x}$$
$$=0 \tag{14}$$

$$-I_\varphi\ddot{u}_{o,x}-(I_{z_sq}-I_{y_sr})\ddot{v}_o+(I_{y_sq}+I_{z_sr})\ddot{w}_o+(I_{q^2}+I_{r^2})\ddot{\psi}-I_{\varphi^2}\ddot{\psi}_{,xx}+I_{z\varphi}\ddot{\theta}_{y,x}+I_{y\varphi}\ddot{\theta}_{z,x}-A_{\varphi11}u_{o,xxx}$$
$$-A_{\alpha16}u_{o,xx}-A_{y_s\varphi16}v_{o,xxx}-A_{y_s\alpha66}v_{o,xx}-A_{z_s\varphi16}w_{o,xxx}-A_{z_s\alpha66}w_{o,xx}+A_{\varphi^2}11\psi_{,xxxx}-A_{\alpha^2}66\psi_{,xx}-B_{\varphi11}\theta_{y,xxx}$$
$$-(B_{\alpha16}+A_{z_s\varphi16})\theta_{y,xx}-A_{z_s\alpha66}\theta_{y,x}-\underline{B}_{\varphi11}\theta_{z,xxx}-(\underline{B}_{\alpha16}+A_{y_s\varphi16})\theta_{z,xx}-A_{y_s\alpha66}\theta_{z,x}$$
$$=0 \tag{15}$$

$$I_1\ddot{u}_o+I_2\ddot{\theta}_y+\widetilde{I}_2\ddot{\theta}_z-I_{z\varphi}\ddot{\psi}_{,x}-B_{11}u_{o,xx}+A_{z_s16}u_{o,x}-B_{y_s16}v_{o,xx}+(A_{y_sz_s66}+A_{z_sz_n55})v_{o,x}-B_{z_s16}w_{o,xx}$$
$$+(A_{z_s^2}66+A_{y_sz_n55})w_{o,x}+B_{\varphi11}\psi_{,xxx}-(A_{z_s\varphi16}+B_{\alpha16})\psi_{,xx}+A_{z_s\alpha66}\psi_{,x}-D_{11}\theta_{y,xx}+(A_{z_s^2}66+A_{z_n^2}55)\theta_y$$
$$-\widetilde{D}_{11}\theta_{z,xx}-(B_{y_s16}-\underline{B}_{z_s16})\theta_{z,x}+(A_{y_sz_s66}+A_{y_nz_n55})\theta_z$$
$$=0 \tag{16}$$

$$\underline{I}_1\ddot{u}_o-I_{y\varphi}\ddot{\psi}_{,x}+\widetilde{I}_2\ddot{\theta}_y+\underline{I}_2\ddot{\theta}_z-\underline{B}_{11}u_{o,xx}+A_{y_s16}u_{o,x}-\underline{B}_{y_s16}v_{o,xx}+(A_{y_s^2}66+A_{z_sy_n55})v_{o,x}-\underline{B}_{z_s16}w_{o,xx}$$
$$+(A_{z_s^2}66-A_{y_sy_n55})w_{o,x}+\underline{B}_{\varphi11}\psi_{,xxx}-(A_{y_s\varphi16}+\underline{B}_{\alpha16})\psi_{,xx}+A_{y_s\alpha66}\psi_{,x}-\widetilde{D}_{11}\theta_{y,xx}-(\underline{B}_{z_s16}-B_{y_s16})\theta_{y,x}$$
$$+(A_{z_sy_s66}+A_{z_ny_n55})\theta_y-\underline{D}_{11}\theta_{z,xx}+(A_{y_sz_s66}+A_{y_nz_n55})\theta_z$$
$$=0 \tag{17}$$

The nomenclature for the stiffness constants used are

$$\left[A_{f(s,n)ij}\quad B_{f(s,n)ij}\quad \underline{B}_{f(s,n)ij}\quad D_{f(s,n)ij}\quad \underline{D}_{f(s,n)ij}\quad \widetilde{D}_{f(s,n)ij}\right]=\int_s\int_n\overline{Q}_{ij}f(s,n)[1,z,y,z^2,y^2,yz]\,\mathrm{d}s\,\mathrm{d}n \tag{18}$$

where

$$f(s,n)\in[1,z_s,y_s,z_n,y_n,r,q,\varphi,(r-\varphi_{,s})]$$

Here $(r-\varphi_{,s})$ is taken equal to α.

Similarly, the inertial constants can be written as

$$\left[I_o\quad I_1\quad \underline{I}_1\quad I_2\quad \underline{I}_2\quad \widetilde{I}_2\quad I_{f(s,n)}\right]=\int_s\int_n\rho[1,z,y,z^2,y^2,yz,f(s,n)]\,\mathrm{d}s\,\mathrm{d}n$$

The essential six forced boundary conditions obtained by the Hamilton's principle, are

$$A_{11}u_{o,x}+A_{y_s16}v_{o,x}+A_{z_s16}w_{o,x}-A_{\varphi11}\psi_{,xx}+A_{\alpha16}\psi_{,x}+B_{11}\theta_{y,x}+A_{z_s16}\theta_y+\underline{B}_{11}\theta_{z,x}+A_{y_s16}\theta_z=P \tag{19}$$

$$A_{y_s16}u_{o,x}+(A_{y_s^2}66+A_{z_s^2}55)v_{o,x}+(A_{z_sy_s66}+A_{z_sy_s55})w_{o,x}-A_{y_s\varphi16}\psi_{,xx}+A_{y_s\alpha66}\psi_{,x}+B_{y_s16}\theta_{y,x}$$
$$+(A_{z_sy_s66}+A_{z_sz_n55})\theta_y+\underline{B}_{y_s16}\theta_{z,x}+(A_{y_s^2}66+A_{y_nz_s55})\theta_z=V_y \tag{20}$$

$$A_{z_s16}u_{o,x}+(A_{y_sz_s66}-A_{y_sz_s55})v_{o,x}+(A_{z_s^2}66+A_{y_s^2}55)w_{o,xx}-A_{z_s\varphi16}\psi_{,xx}+A_{z_s\alpha66}\psi_{,x}+B_{z_s16}\theta_{y,x}$$
$$+(A_{z_s^2}66-A_{y_sz_n55})\theta_y+\underline{B}_{z_s16}\theta_{z,x}+(A_{y_sz_s66}-A_{y_ny_s55})\theta_z=V_z \tag{21}$$

$$A_{\varphi 11}u_{o,xx} + A_{\alpha 16}u_{o,x} + A_{y_s\varphi 16}v_{o,xx} + A_{y_s\alpha 66}v_{o,x} + A_{z_s\varphi 16}w_{o,xx} + A_{z_s\alpha 66}w_{o,x} - A_{\varphi^2 11}\psi_{,xxx} + A_{\alpha^2 66}\psi_{,x} + B_{\varphi 11}\theta_{y,xx} + (B_{\alpha 16} + A_{z_s\varphi 16})\theta_y, x + A_{z_s\alpha 66}\theta_y + \underline{B}_{\varphi 11}\theta_{z,xx} + (\underline{B}_{\alpha 16} + A_{y_s\alpha 66})\theta_z = T \tag{22}$$

$$B_{11}u_{o,x} + B_{y_s 16}v_{o,x} + B_{z_s 16}w_{o,x} - B_{\varphi 11}\psi_{,xx} + B_{\alpha 16}\psi_{,x} + D_{11}\theta_{y,x} + B_{z_s 16}\theta_y + \widetilde{D}_{11}\theta_{z,x} + B_{y_s 16}\theta_z = M_y \tag{23}$$

$$\underline{B}_{11}u_{o,x} + \underline{B}_{y_s 16}v_{o,x} + \underline{B}_{z_s 16}w_{o,x} - \underline{B}_{\varphi 11}\psi_{,xx} + \underline{B}_{\alpha 16}\psi_{,x} + \widetilde{D}_{11}\theta_{y,x} + \underline{B}_{z_s 16}\theta_y + \underline{D}_{11}\theta_{z,xx} + \underline{B}_{y_s 16}\theta_z = M_z \tag{24}$$

These governing equation and the associated boundary conditions will be used for stiffness matrix formulation. This is done by assuming appropriate polynomials for the displacement field based on the order of the static part of the differential equation and substituting these back into the governing equation. In this process certain constants can be eliminated and at the same time, certain constant become dependent on material and sectional properties. The details of the formulation is given in the next section.

3. Finite element formulation

The finite element formulation begins by assuming the interpolating functions of appropriate order for the six degrees of freedom. Looking at the governing equations (Eqs. (12)–(17)), we see that the axial displacement (u_o) and the slopes about y- and z-axis (θ_y and θ_z) require quadratic polynomial, while the lateral and transverse displacement (v_o and w_o) and the twist (ψ) degrees of freedom require cubic polynomials. Hence the interpolating polynomials for the six degrees of freedom can be assumed as

$$\begin{aligned} u_o(x) &= a_1 + a_2x + a_3x^2 \\ v_o(x) &= a_4 + a_5x + a_6x^2 + a_7x^3 \\ w_o(x) &= a_8 + a_9x + a_{10}x^2 + a_{11}x^3 \\ \psi(x) &= a_{12} + a_{13}x + a_{14}x^2 + a_{15}x^3 \\ \theta_y(x) &= a_{16} + a_{17}x + a_{18}x^2 \\ \theta_z(x) &= a_{19} + a_{20}x + a_{21}x^2 \end{aligned} \tag{25}$$

In all, there are 21 constants to be evaluated. However there are only 12 boundary conditions (six at each node, see Fig. 2). Hence there are nine constants which are not independent. These can be eliminated by substituting the assumed displacement field in the governing equations (Eqs. (12)–(17)). Here we introduce two vectors $\{a\}$ and $\{a_u\}$, where $\{a\}$ containing all the unknown constants and $\{a_u\}$ is the vector containing the dependent constants. These can be written as

$$\begin{aligned} \{a\} &= \{a_1, a_2, a_4, a_5, a_8, a_9, a_{12}, a_{13}, a_{16}, a_{17}, a_{19}, a_{20}\} \\ \{a_u\} &= \{a_3, a_6, a_7, a_{10}, a_{11}, a_{14}, a_{15}, a_{18}, a_{21}\} \end{aligned} \tag{26}$$

First the assumed displacement field (Eq. (25)) is substituted in the six coupled governing differential equation. This process enables to isolate the dependent constants $\{a_u\}$ from total number of constants $\{a\}$. That is the vector $\{a_u\}$ is expressed in terms of vector $\{a\}$, through a transformation matrix. This can be done as follows. On substitution of assumed displacement field in governing equation, the constants $\{a_u\}$ can be expressed in terms of $\{a\}$ as

$$[A_1]\{a_u\} = [A_2]\{a\} \quad \text{or} \quad \{a_u\} = [A]\{a\} \quad \text{where } [A] = [A_1]^{-1}[A_2] \tag{27}$$

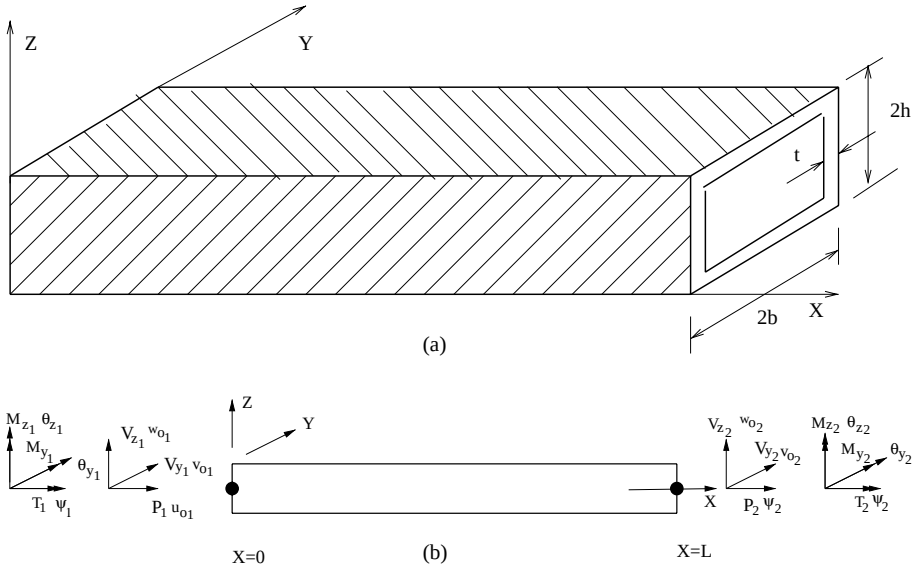

Fig. 2. (a) Thin walled box beam element and (b) nodal displacements and nodal forces.

$[A_1]$ is of size 9×9 while $[A_2]$ is of size 9×12. One can see that these constants are functions of material and cross-sectional properties of the thin walled beam. The explicit form of matrices $[A_1]$ and $[A_2]$ are given in Appendix A. The matrix $[A]$ in Eq. (27) is evaluated by computing the inverse of matrix $[A_1]$, numerically. On substitution of Eq. (27) in the governing equation (Eqs. (12)–(17)) the assumed polynomials for the six displacement field can be written as

$$
\begin{aligned}
u_o(x) &= [1\ \ x\ \ 0\ \ 0\ \ 0\ \ 0\ \ 0\ \ 0\ \ 0\ \ 0\ \ 0\ \ 0]\{a\} + [x^2\ \ 0\ \ 0\ \ 0\ \ 0\ \ 0\ \ 0\ \ 0\ \ 0][A]\{a\}\\
v_o(x) &= [0\ \ 0\ \ 1\ \ x\ \ 0\ \ 0\ \ 0\ \ 0\ \ 0\ \ 0\ \ 0\ \ 0]\{a\} + [0\ \ x^2\ \ x^3\ \ 0\ \ 0\ \ 0\ \ 0\ \ 0\ \ 0][A]\{a\}\\
w_o(x) &= [0\ \ 0\ \ 0\ \ 0\ \ 1\ \ x\ \ 0\ \ 0\ \ 0\ \ 0\ \ 0\ \ 0]\{a\} + [0\ \ 0\ \ 0\ \ x^2\ \ x^3\ \ 0\ \ 0\ \ 0\ \ 0][A]\{a\}\\
\psi(x) &= [0\ \ 0\ \ 0\ \ 0\ \ 0\ \ 0\ \ 1\ \ x\ \ 0\ \ 0\ \ 0\ \ 0]\{a\} + [0\ \ 0\ \ 0\ \ 0\ \ 0\ \ x^2\ \ x^3\ \ 0\ \ 0][A]\{a\}\\
\theta_y(x) &= [0\ \ 0\ \ 0\ \ 0\ \ 0\ \ 0\ \ 0\ \ 0\ \ 1\ \ x\ \ 0\ \ 0]\{a\} + [0\ \ 0\ \ 0\ \ 0\ \ 0\ \ 0\ \ 0\ \ x^2\ \ 0][A]\{a\}\\
\theta_z(x) &= [0\ \ 0\ \ 0\ \ 0\ \ 0\ \ 0\ \ 0\ \ 0\ \ 0\ \ 0\ \ 1\ \ x]\{a\} + [0\ \ 0\ \ 0\ \ 0\ \ 0\ \ 0\ \ 0\ \ 0\ \ x^2][A]\{a\}
\end{aligned}
\tag{28}
$$

The first task is to express the unknown coefficients in terms of the nodal displacement vector $\{u\}_e$ which is ordered as

$$\{u\}_e = \{u_{o_1},\ v_{o_1},\ w_{o_1},\ \psi_1,\ \theta_{y_1},\ \theta_{z_1},\ u_{o_2},\ v_{o_2},\ w_{o_2},\ \psi_2,\ \theta_{y_2},\ \theta_{z_2}\}^{\mathrm{T}}$$

where u_{o_1}, u_{o_2}, v_{o_1}, v_{o_2} and w_{o_1}, w_{o_2} are the axial, lateral and transverse displacements at two nodes while ψ_1, ψ_2, θ_{y_1}, θ_{y_2} and θ_{z_1}, θ_{z_2} are the respective slopes at the two nodes. This is done by substituting $x = 0$ and $x = L$ in Eq. (28), which can be written in matrix form as

$$\{u\}_e = [R]\{a\}$$

Inverting the above equation, we get

$$\{a\} = [R]^{-1}\{u\}_e = [B]\{u\}_e \tag{29}$$

Using the above equation in Eq. (28), we can write all the displacement field in terms of its nodal quantities, which constitute the shape function of the displacement field. Thus

$$\{u\} = [N]\{u\}_e, \quad [N] = [\,N_u \quad N_v \quad N_w \quad N_\psi \quad N_{\theta_y} \quad N_{\theta_z}\,] \tag{30}$$

where $[\,N_u \quad N_v \quad N_w \quad N_\psi \quad N_{\theta_y} \quad N_{\theta_z}\,]$ are the shape functions corresponding to the six displacement fields.

Next the six force boundary condition (Eqs. (19)–(24)) are considered and expressed in terms of nodal force quantities. That is at $x = 0$, we have $P(0) = -P_1$, $V_y(0) = -V_{y1}$, $V_z(0) = -V_{z1}$, $T(0) = -T_1$, $M_y(0) = -M_{y1}$ and $M_z(0) = -M_{z1}$ and at $x = L$, we have $P(L) = P_2$, $V_y(L) = V_{y2}$, $V_z(L) = V_{z2}$, $T(L) = T_2$, $M_y(L) = M_{y2}$ and $M_z(L) = M_{z2}$. Substituting these in Eqs. (19)–(24), we can write the nodal force vector as

$$\{F\} = [C]\{a\} \tag{31}$$

Substituting for $\{a\}$ from Eq. (29), we can write

$$\{F\} = [C][B]\{u\}_e \Rightarrow \{F\} = [K]\{u\}_e \tag{32}$$

where $[K]$ is the exact stiffness matrix, that is derived from the polynomials which exactly satisfy the governing differential equation.

The consistent mass matrix is formulated using the material dependent shape functions (Eq. (30)). That is

$$[M] = \int_0^L \int_A \rho [N]^{\mathrm{T}} [N] \,\mathrm{d}n \,\mathrm{d}s \tag{33}$$

Substituting Eq. (30), expanding and integrating, the mass matrix can be written as

$$\begin{aligned}
[M] = {} & I_o \int_0^L [N_u]^{\mathrm{T}}[N_u]\,\mathrm{d}x + (I_{z_s^2} + I_{y_s^2}) \int_0^L ([N_v]^{\mathrm{T}}[N_v] + [N_w]^{\mathrm{T}}[N_w])\,\mathrm{d}x - (I_{z_s q} - I_{y_s r}) \int_0^L ([N_v]^{\mathrm{T}}[N_\psi] \\
& + [N_\psi]^{\mathrm{T}}[N_v])\,\mathrm{d}x + (I_{z_s r} + I_{y_s q}) \int_0^L ([N_w]^{\mathrm{T}}[N_\psi] + [N_\psi]^{\mathrm{T}}[N_w])\,\mathrm{d}x + (I_{r^2} + I_{q^2}) \int_0^L [N_\psi]^{\mathrm{T}}[N_\psi]\,\mathrm{d}x \\
& + I_2 \int_0^L [N_{\theta_y}]^{\mathrm{T}}[N_{\theta_y}]\,\mathrm{d}x + \underline{I}_2 \int_0^L [N_{\theta_z}]^{\mathrm{T}}[N_{\theta_z}]\,\mathrm{d}x + \underline{I}_1 \int_0^L ([N_{\theta_z}]^{\mathrm{T}}[N_u] + [N_u]^{\mathrm{T}}[N_{\theta_z}])\,\mathrm{d}x \\
& + I_1 \int_0^L ([N_{\theta_y}]^{\mathrm{T}}[N_u] + [N_u]^{\mathrm{T}}[N_{\theta_y}])\,\mathrm{d}x + \widetilde{I}_2 \int_0^L ([N_{\theta_y}]^{\mathrm{T}}[N_{\theta_z}] + [N_{\theta_z}]^{\mathrm{T}}[N_{\theta_y}])\,\mathrm{d}x + I_{1\varphi} \int_0^L ([N_{\theta_y}]^{\mathrm{T}}[N_{\psi_x}] \\
& - [N_{\theta_{y_x}}]^{\mathrm{T}}[N_\psi])\,\mathrm{d}x + \underline{I}_{1\varphi} \int_0^L ([N_{\theta_z}]^{\mathrm{T}}[N_{\psi_x}] - [N_{\theta_{z_x}}]^{\mathrm{T}}[N_\psi])\,\mathrm{d}x - I_\varphi \int_0^L ([N_u]^{\mathrm{T}}[N_{\psi_x}] \\
& - [N_\psi]^{\mathrm{T}}[N_{u_x}])\,\mathrm{d}x - I_{\varphi^2} \int_0^L [N_\psi]^{\mathrm{T}}[N_{\psi_{xx}}]\,\mathrm{d}x
\end{aligned} \tag{34}$$

Depending on the geometry of the cross-section, many of the constant in the mass matrix formulated above vanishes resulting in a simpler form.

4. Numerical experiments

The formulated element has super convergent property as it uses exact solution to the governing equation as its interpolation function. Hence, for point loads, one element between any two discontinuities is sufficient to capture the exact response for static analysis. This results in substantial reduction in the

system size. For dynamic analysis, consistent mass matrix formulated based on the above interpolation functions are used. As a result, for a given discretization, the accuracy of the present formulation is expected to be superior compared to elements formulated based on conventional polynomial approximation. This is because, the stiffness of the structure is exactly represented even though the inertial distribution is approximate. Hence, good accuracy in dynamic analysis can be expected from this element using smaller system sizes. The performance of the formulated element is examined for static, free vibration and wave propagation problems.

Static and dynamic analyses of different box-beam, I-beam and rectangular flat beam section of increasing complexities are performed. The beam configurations used in the experimentation is chosen to have different material properties and ply layup sequences. Static and free vibration results are compared with experimental, analytical and numerical results available in the literature.

The performance of the element for wave propagation problems can be judged by it's ability to capture higher order modes with very small system size. Hence, the numerical experiments for dynamic analysis is so designed that, first the ability of the formulated element to accurately capture higher order modes is examined before it's use in wave propagation problems, where the frequency content of forcing function is usually very high. The main aim of this numerical experiment is to show the effect of shear deformation (in FSDT) on the overall transverse response in a box beam. In addition, simultaneous existence of various propagating modes is graphically captured.

4.1. Static analysis

Static analysis is done for AS4/3501-6 graphite-epoxy box beams with three different symmetric and antisymmetric ply layup sequences to test the performance of the formulated element. The response of these cantilever beams of length 0.762 m. under unit static loads at the free end were experimentally investigated by Chandra et al. (1990). The material properties and ply layup are provided in Tables 1 and 2 respectively. The symmetric configuration $[\theta]_S$ exhibit bending-torsion and extension-shear coupling while the antisymmetric configuration exhibit extension–torsion coupling. Figs. 3 and 4 show the induced twist due to tip bending load and induced bending slope due to tip torque of a $[45]_S$ beam respectively, as a function of spanwise coordinates. In both the cases, the present result correlates well with experimental data and the tip deflection converges using just one element confirming the exactness of the stiffness matrix. In Fig. 3, the result from the formulated element is also compared with the finite element analysis VABS by Cesnik and Hodges (1997) and analytical solutions by Berdichevsky et al. (1992) and Smith and Chopra (1991). In Figs. 5 and 6 the effective torsional stiffnesses are presented for symmetric and antisymmetric sections respec-

Table 1
Properties of AS4/3501-6 graphite-epoxy ($[\theta]_S$ and $[\theta]_{AS}$) box-beams

Material properties	
E_{11}, psi (GPa)	20.59×10^6 (141.9)
E_{22}, psi (GPa)	1.42×10^6 (9.78)
$G_{12} = G_{13}$, psi (GPa)	0.89×10^6 (6.13)
G_{23}, psi (GPa)	0.696×10^6 (4.80)
ν_{12}	0.42
ρ	0.05224 lb/in^3 (1449 kg/m^3)
Dimensions	
Width ($= 2b$), in. (mm)	0.953 (24.21)
Depth ($= 2h$), in. (mm)	0.53 (13.46)
Ply Thickness ($= t$), in. (mm)	0.005 (0.127)
No. of ply in each side	6

Table 2
Ply layup of AS4/3501-6 graphite-epoxy ($[\theta]_S$ and $[\theta]_{AS}$) box-beams

Beam configuration	Top flange	Bottom flange	Left web	Right web
Symmetric $[\theta]_S$				
$[15]_S$	$[15]_6$	$[15]_6$	$[15/-15]_3$	$[15/-15]_3$
$[30]_S$	$[30]_6$	$[30]_6$	$[30/-30]_3$	$[30/-30]_3$
$[45]_S$	$[45]_6$	$[45]_6$	$[45/-45]_3$	$[45/-45]_3$
Antisymmetric $[\theta]_{AS}$				
$[15]_{AS}$	$[15]_6$	$[-15]_6$	$[15]_6$	$[-15]_6$
$[30]_{AS}$	$[0/30]_3$	$[0/-30]_3$	$[0/30]_3$	$[0/-30]_3$
$[45]_{AS}$	$[0/45]_3$	$[0/-45]_3$	$[0/45]_3$	$[0/-45]_3$

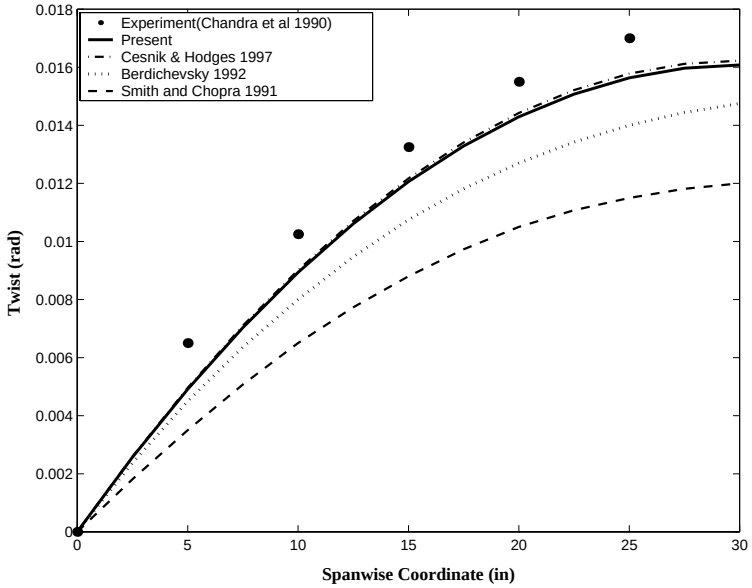

Fig. 3. Induced twist of $[45]_S$ box-beam due to unit tip bending load.

tively. Comparisons provided with experimental results and analytically evaluated cross-sectional stiffnesses by Jung et al. (2002), show good correlation with results generated from the single formulated element.

Cantilever graphite-epoxy I-beam having material properties as given in Table 1 (except $G_{23} = 0.89 \times 10^6$ psi) and sectional dimension of 1.0 in. $\times$ 0.5 in. are experimented for static response. Ply layup sequence is $[(0°/90°)_3/(15°)_2]_f$ for both the flanges, with 15° being the fiber orientation at the top two plies and $[(0°/90°)_4]_w$ for the web. This I-beam is well studied both experimentally and theoretically as open section cases and details of the configuration are given in Chandra and Chopra (1991). These beam has warping restrain effect at the ends and exhibit substantial increase in torsional rigidity according to Vlasov effect. Fig. 7 shows the tip twist due to unit torsional load applied at the tip and the induced twist due to unit bending load at tip. Comparisons are provided with the analytical results presented by Chandra and Chopra (1991) and numerical results provided by Yu et al. (2002) using VABS. Good correlation is observed in both the cases. The tip twists obtained using classical or St. Venant's theory are presented to show the predominant effect of restrained warping on the torsional behavior of open cross-section beams.

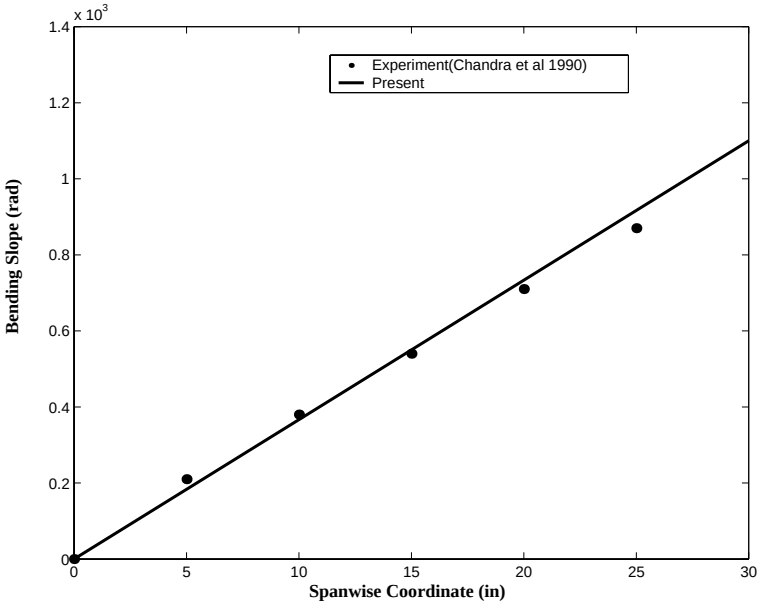

Fig. 4. Induced bending slope of $[45]_S$ box-beam due to unit tip torque.

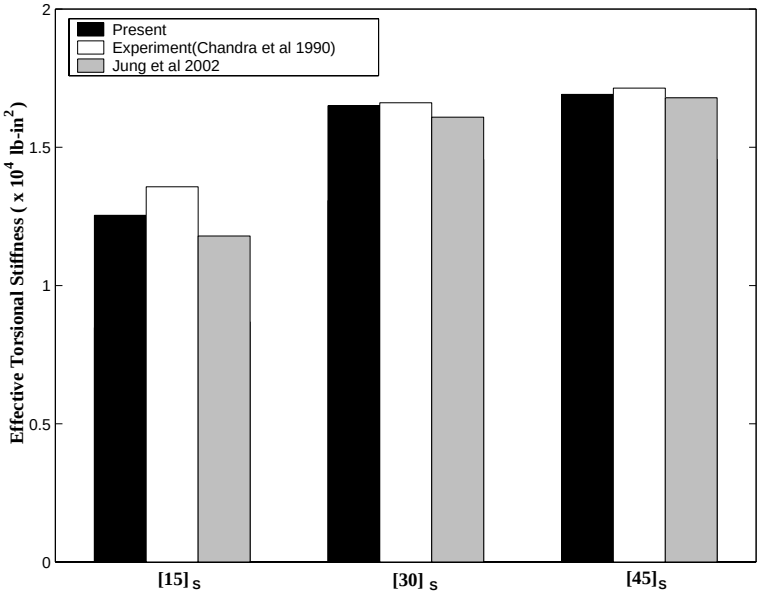

Fig. 5. Effective torsional stiffness of symmetric $[\theta]_S$ box-beams.

4.2. Free vibration analysis

Natural frequencies of a rectangular flat graphite epoxy beam of 30° ply orientation with bending torsion coupling are evaluated and compared with available experimental and theoretical results in Table 3.

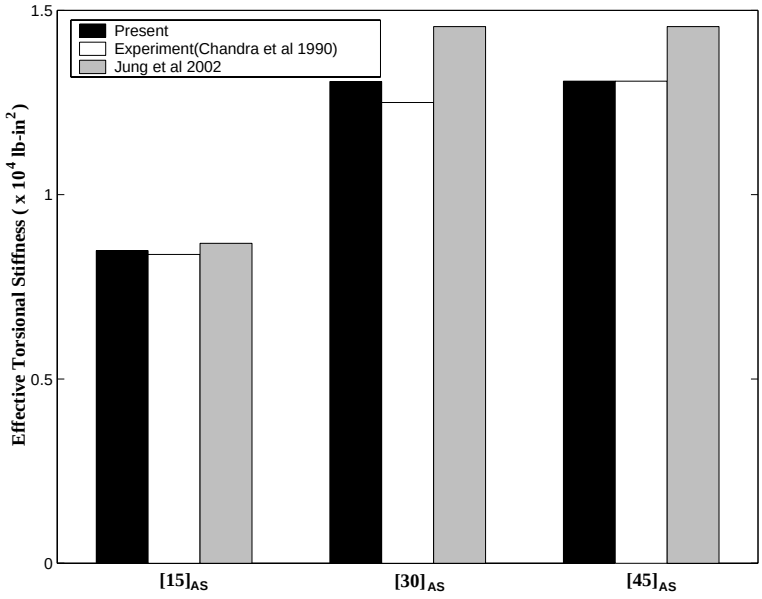

Fig. 6. Effective torsional stiffness of antisymmetric $[\theta]_{AS}$ box-beams.

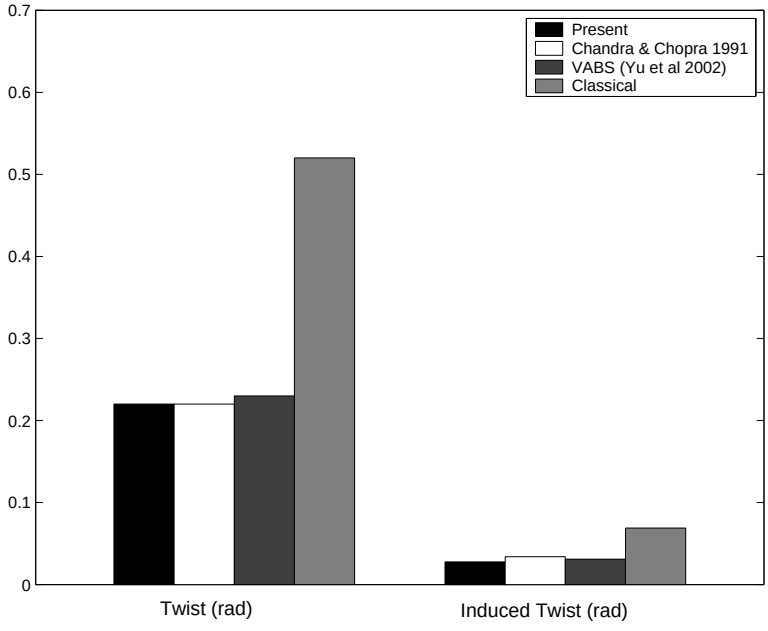

Fig. 7. Twist and induced twist due to unit torsional and bending load at tip of $[(0°/90°)_3/(15°)_2]_f$ and $[(0°/90°)_4]_w$ I-beam.

The beam has a width of 12.7 mm, thickness 3.175 mm and length 190 mm. Material properties are given in Table 4. ST and TS represent spanwise bending-torsion mode with bending and torsion being predominant

Table 3
Natural frequencies (Hz) of 30° graphite epoxy rectangular flat beam

Mode	Abarcar and Cuniff (1972)		Suresh and Nagaraj (1996)	Hodges et al. (1991)	Stemple and Lee (1989)	Jung et al. (2001)	Present
	Experiment	Analysis					
1 (ST)	52.7	52.7	52.6	49.0	53.8	52.7	52.8
2 (C)	–	–	–	195.6	214.1	210.7	210.0
3 (ST)	331.8	329.3	329.1	307.9	335.9	329.2	329.5
4 (ST)	924.7	915.9	918.0	869.1	941.1	918.6	916.1
5 (C)	–	–	–	1215.2	1315.7	1320.4	1263.9
6 (ST)	1766.9	1767.0	1777.3	–	1707.0	1762.9	1756.0
7 (TS)	1827.4	1896.5	1891.6	1660.9	1881.1	1836.6	1858.0
8 (TS)	2984.0	2901.4	2929.9	–	3154.1	2944.6	2909.6

ST and TS represent spanwise bending-torsion mode with bending and torsion being predominant respectively and C is the chordwise bending mode.

Table 4
Material properties of graphite-epoxy rectangular flat beam

Material properties	
E_{11}, psi (GPa)	18.73×10^6 (129.1)
E_{22}, psi (GPa)	1.364×10^6 (9.408)
G_{12}, psi (GPa)	0.7479×10^6 (5.157)
G_{23}, psi (GPa)	0.3686×10^6 (2.541)
G_{23}, psi (GPa)	0.6242×10^6 (4.304)
ν_{12}	0.3
ρ	0.056 lb/in^3 (1551 kg/m^3)

respectively and C is the chordwise bending mode. Free vibration results for the beam was obtained experimentally by Abarcar and Cuniff (1972), analytically by Abarcar and Cuniff (1972) and Suresh and Nagaraj (1996) and a finite element analysis by Stemple and Lee (1989). Jung et al. (2001) evaluated the cross-sectional stiffness analytically and used 20 degrees of freedom beam elements to obtain the dynamic characteristics. Results presented by Hodges et al. (1991) was derived from finite element cross-sectional model using NABSA (Non Homogeneous Anisotropic Beam Section Analysis) and beam finite elements for lengthwise discretization. The present results obtained using only 10 elements with a total of 60 degrees of freedom, show good correlation with the available results from the literature.

Chandra and Chopra (1992) performed free vibration experiments for non-rotating AS4/3501-6 graphite epoxy box beams ($[\theta]_S$ and $[\theta]_{AS}$) whose properties are described in Tables 1 and 2, respectively. In Fig. 8 the fundamental frequencies of $[15]_{AS}$, $[30]_{AS}$ and $[45]_{AS}$ are compared with above experimental results. The analytical results were evaluated by Chandra and Chopra (1992) using Galerkin's method. The present results obtained with three formulated beam elements correlate well with available results.

Next, the free vibration behavior of the extension–torsion coupled box beam is investigated for which the material properties and dimensions given in Table 5 is used. The beam has an antisymmetric configuration with [20/−70/20/−70/−70/20] ply layup in each wall. Table 6 gives the bending modes and first two extension–torsion modes frequencies for this beam using the formulated element. The results are compared with those presented by Hodges et al. (1991) using NABSA and TAIL for cross-sectional stiffness analysis. S, C and TE are the spanwise bending, chordwise bending and torsion–extension modes respectively. Frequencies obtained using TAIL requires 16 elements. The present results show good correlation.

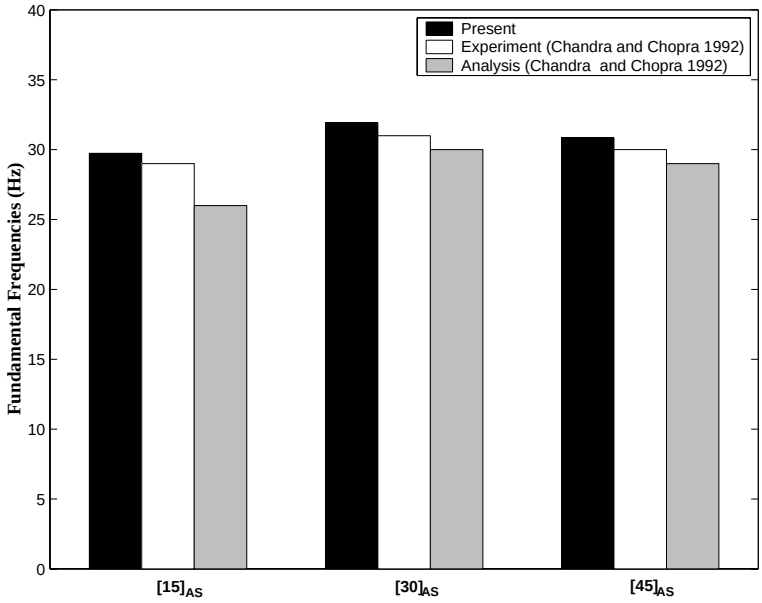

Fig. 8. Fundamental frequencies of antisymmetric $[\theta]_{AS}$ box-beams.

Table 5
Properties of T300/5208 graphite-epoxy box-beam

Material properties	
E_{11}, psi (GPa)	21.3×10^6 (146.79)
E_{22}, psi (GPa)	1.6×10^6 (11.03)
$G_{12} = G_{13}$, psi (GPa)	0.9×10^6 (6.20)
G_{23}, psi (GPa)	0.7×10^6 (4.82)
ν_{12}	0.28
ρ	0.05764 lb/in^3 (1599 kg/m^3)
Dimensions	
Width ($= 2b$), in. (mm)	1.32 (33.53)
Depth ($= 2h$), in. (mm)	0.66 (16.76)
Ply Thickness ($= t$), in. (mm)	0.0055 (0.1397)
Length in. (mm)	100 (2540)

Table 6
Natural frequencies (Hz) of T300/5208 graphite epoxy box-beam

Mode	Hodges et al. (1991)		Present (No. of Elements)					
	NABSA	TAIL	2	3	5	10	15	20
1 (S)	3.00	3.09	3.05	3.05 (0.0%)	3.05	3.07	3.08	3.09
2 (C)	5.19	5.74	5.57	5.56 (−0.18%)	5.56	5.57	5.58	5.59
3 (S)	19.04	19.64	19.25	19.17 (−0.42%)	19.12	19.19	19.28	19.36
4 (C)	32.88	36.39	35.05	34.87 (−0.52%)	34.78	34.81	34.88	34.98
5 (S)	54.65	56.36	65.12	54.04	53.62	53.65 (0.06%)	53.89	54.12
6 (C)	93.39	103.29	118.58	98.07	97.13	96.90 (−0.24%)	97.08	97.34
1 (TE)	180.32	177.23	178.76	176.25	174.98	174.44 (−0.31%)	174.34	174.30
2 (TE)	544.47	535.15	606.68	576.44	542.27	527.62	524.93 (−0.51%)	523.98

S, C and TE are the spanwise bending, chordwise bending and torsion–extension modes respectively.

As stated earlier and validated by the static analysis examples, the present formulation derives the exact elemental stiffness matrix using higher order shape functions. Though the mass modeling is not exact and a consistent mass matrix using the derived interpolating polynomials is formulated for dynamic analysis, the present beam element is expected to exhibit improved convergence. In Table 6 the natural frequencies obtained corresponding to the number of elements used are also presented, to illustrate the super convergent properties of the formulated element. The percentage values given in the parenthesis give the change in the frequencies due to mesh refinement. It is observed that the frequencies corresponding to the first four bending modes nearly converges after two elements with a maximum difference of 0.52% at the fourth frequency obtained using three elements.

Next, the ability of the element to capture higher modes with smaller system size, is investigated. This is very crucial for the wave propagation analysis (treated next), where the frequency content is very high and as a result all the higher order modes participate in the response.

An asymmetric graphite epoxy box beam configuration ($[0/90]_A$) having material properties and dimensions as in Table 1 is used. The results are compared with 3-D finite element simulation, which is given in Table 7. The beam has a ply orientation of $[0_3/90_3]$ and $[90_3/0_3]$ in top and bottom flanges and similar in left and right webs. Asymmetry in ply layup sequences produces extension shear coupling. The 3-D finite element results are obtained using ANSYS general purpose program where eight noded brick element is used to model the structure The model has a total of 15128 nodes and 3×15128 degrees of freedom. The relative difference in the 14th and 15th frequency obtained using a finer 3-D mesh of 20008 nodes and 3×20008 degrees of freedom is 0.5%. Thus no further mesh refinement is done. The system size required by the present element is 30×6. Frequencies with and without transverse shear are presented. The EBT (without transverse shear) formulation is derived from present FSDT (with transverse shear) by considering the stiffness constants i.e. $A_{f(s,n)55}$ (see Eq. (18)) corresponding to transverse shear to be infinite. Bending and extensional frequencies shows good correlations and the effect of transverse shear is more prominent at higher frequencies.

4.3. Wave propagation problem

In wave propagation the frequency content of the exciting force is very high. The response of the structure to such loading extracts the participation of all the higher modes. Smaller element size is required to match the small wavelengths at higher frequencies. This results in finer finite element modeling producing

Table 7
Natural frequencies (Hz) of AS4/3501-6 graphite epoxy $[0/90]_A$ box-beam

Mode	Present		3-D FEM
	With transverse shear	Without transverse shear	
1 (S)	31.02	31.06	30.99
2 (C)	49.17	49.34	49.19
3 (S)	192.55	194.57	187.22
4 (C)	301.63	308.75	298.13
6 (S)	531.18	473.02	494.34
7 (C)	817.54	862.40	794.24
11 (S)	1642.38	1757.35	1680.8
12 (E)	2107.28	2107.33	2111.7
14 (S)	2381.89	2619.31	2349.4
15 (C)	2409.78	2771.02	2418.0
16 (S)	3220.05	3321.34	3198.0

S and C are the spanwise and chordwise bending modes respectively.

large system size. The amount of literature available for such wave propagation problems specially for box beams is very scarce and to the author's best knowledge can be said almost non-existent. In such situation, it is necessary to examine the ability of the element to capture all the higher order modes in a model having smaller system size. This was done in the previous example of the free vibration analysis section. The main objectives here are the following: (1) To study the fundamental aspects of wave propagation in shear flexible box beam as opposed to elementary box beam. (2) To graphically capture the various propagating

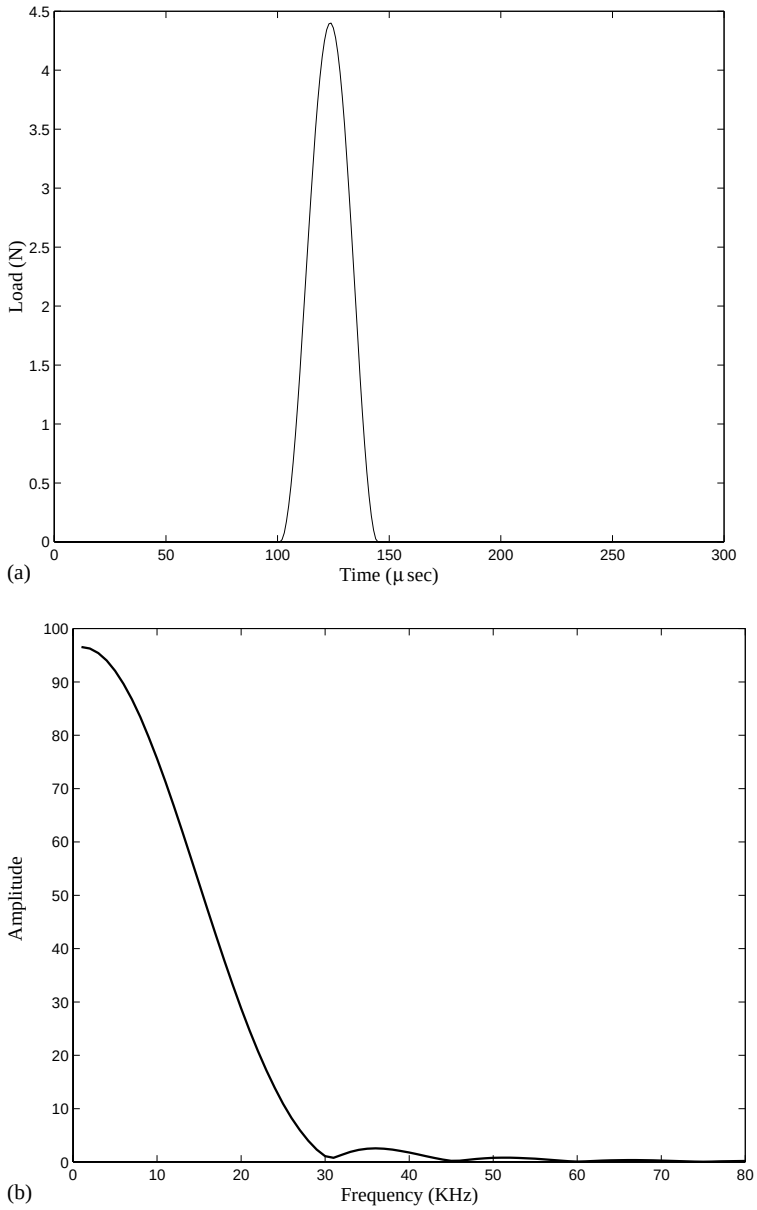

Fig. 9. (a) Impact load and (b) Fourier transform of load.

wave modes in a symmetric/antisymmetric box beam due to either bending-shear-torsion coupling or extension-shear-torsion coupling. This feature, coupled with some of the fundamental aspects of wave propagation in a shear flexible box beam, will enable us to ascertain the accuracy of the solution.

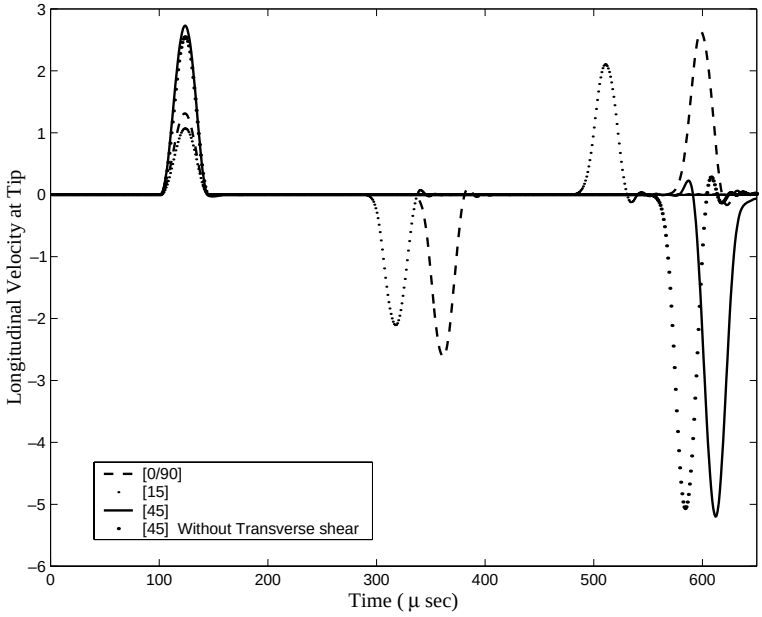

Fig. 10. Longitudinal tip velocities of $[0/90]_A$, $[45]_S$, $[15]_{AS}$ box-beam due to tip impact load.

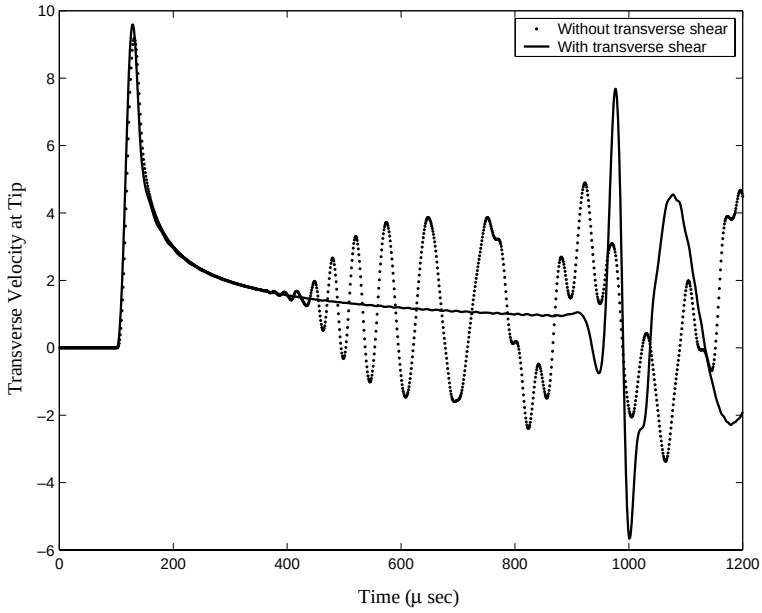

Fig. 11. Transverse tip velocity of a $[0/90]_A$ box-beam due to tip impact load.

4.3.1. Cantilever beam under tip impact load

Numerical experiments are performed on cantilever box beams with different ply orientation both with and without considering the transverse shear effects to study the difference in wave propagation characteristics of EBT and FSD beams.

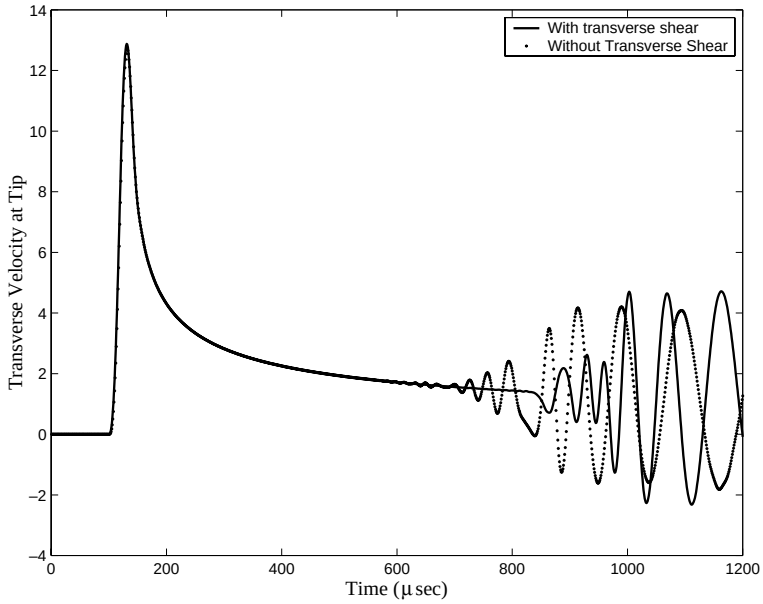

Fig. 12. Transverse tip velocity of a $[45]_S$ box-beam due to tip impact load.

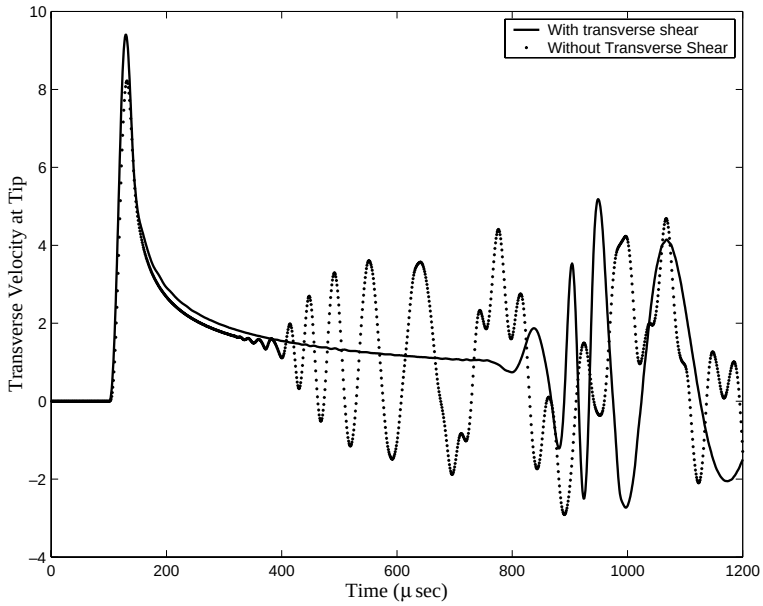

Fig. 13. Transverse tip velocity of a $[15]_{AS}$ box-beam due to impact load.

Three Graphite epoxy cantilever box beams $[0/90]_A$, $[45]_S$, $[15]_{AS}$ with material properties and dimensions as in Table 1 are used for the numerical experiment. The exciting impact load shown in Fig. 9 has an amplitude of 4.4 N and duration is of 50 μs with a very high frequency content of 44 kHz. The beams are modeled with 1000 elements with 1000×6 degrees of freedom, where 6 is the band width. Newmarks time integration is used with time increments of 1 μs.

Fig. 10 shows the longitudinal velocities measured at the tip due to impact load applied also applied at tip in longitudinal direction. The effect of neglecting transverse shear in $[45]_S$ decreases the amplitude of initial response to the load and also increases the velocity with the first reflection occurring around 40 μs earlier than that with transverse shear while in $[0/90]_A$, $[15]_{AS}$ the effect of neglecting transverse shear does not produce any difference This observation is justified as $[45]_S$ beam has a prominent extension shear coupling. Also, it is seen that longitudinal waves in $[0/90]_A$ and $[15]_{AS}$ beam travel much faster than $[45]_S$ beam.

Figs. 11–13 are the transverse velocities at tip due to impact loading applied at tip in transverse direction of $[0/90]_A$, $[45]_S$, $[15]_{AS}$ beams respectively. Neglecting transverse shear increases the velocity in all cases and the effect is most prominent in $[15]_{AS}$. Thus it can be concluded from the observations that FSDT predicts lower wave speeds than EBT.

4.3.2. Response to modulated sinusoidal pulse

The aim of this experiment is to graphically capture various propagating modes in a box beam. Depending on the ply orientation and stacking sequence, various elastic coupling are exhibited in a box beam. The governing equation for the box beam, derived in Section 2 of this paper, showed that it is fourth order in transverse displacements and twist, third order for slopes and axial displacement. Hence waves in such systems are necessarily dispersive, that is the pulse changes its shape as it propagates. In order that all the propagating modes are captured graphically, a pulse that travels non-dispersively is required. For this purpose, a modulated sinusoidal pulse is used. Such a pulse has zero energy at all frequencies other than the frequency at which the sine pulse is excited. Such pulses are extensively used in structural health monitoring studies (Nag et al., 2002; Valdés and Soutis, 2001; Lin and Yuan, 2001). As stated earlier in Section 1, further refinement in the present beam formulation by using improved cross-sectional models are required prior to such applications. This sinusoidal pulse modulated at a high frequency is allowed to propagate through an infinite beam (Fig. 14). The beam is considered infinite in a sense that the boundary reflections can be neglected within the time of observation. The graphite epoxy box beams $[\theta]_{AS}$ and $[\theta]_S$ with material properties and dimensions as in Table 1 are used for this experiment. The modulated pulse is applied at a point C in axial and transverse directions and the axial and transverse velocity are observed at a point D

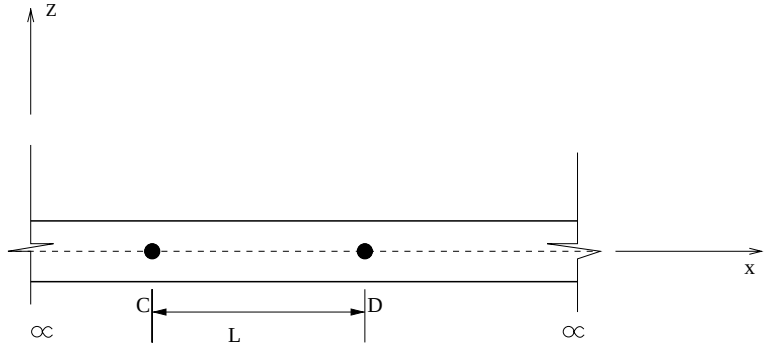

Fig. 14. An infinite box beam to observe non-dispersively propagating modes.

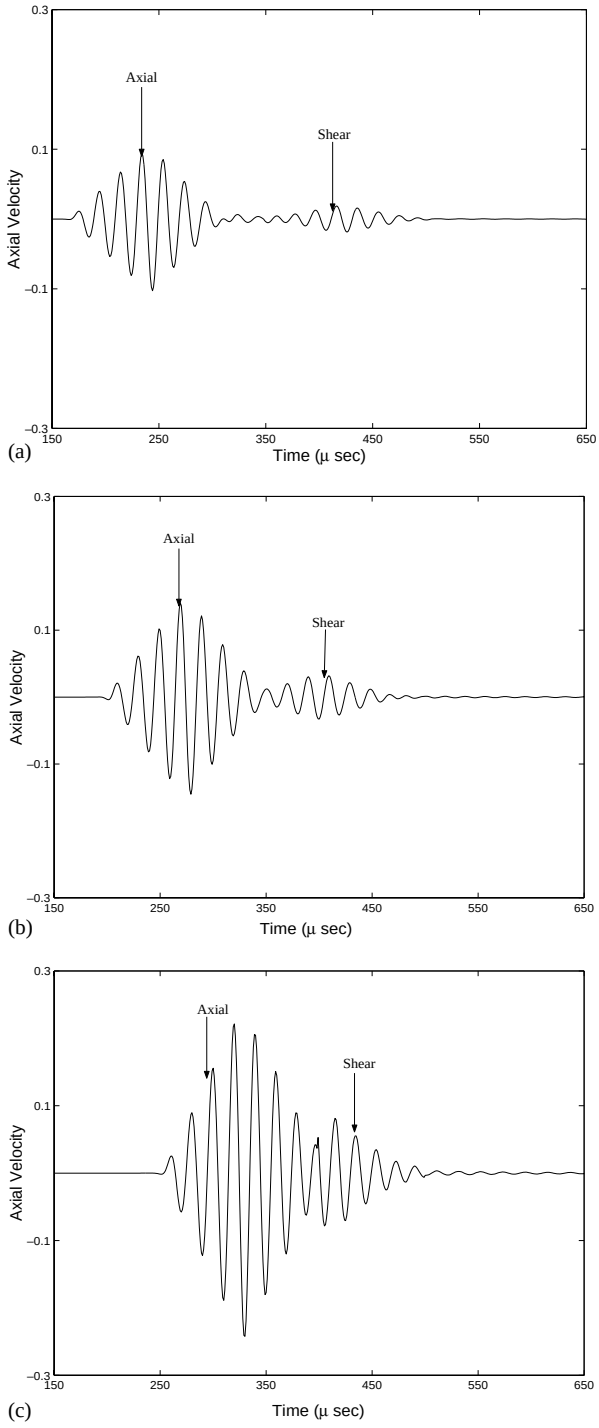

Fig. 15. Axial velocities of (a) $[15]_S$, (b) $[30]_S$, (c) $[45]_S$ box-beam due to a sinusoidal pulse modulated at 50 kHz applied in axial direction. Shear modes are shown in magnified scales.

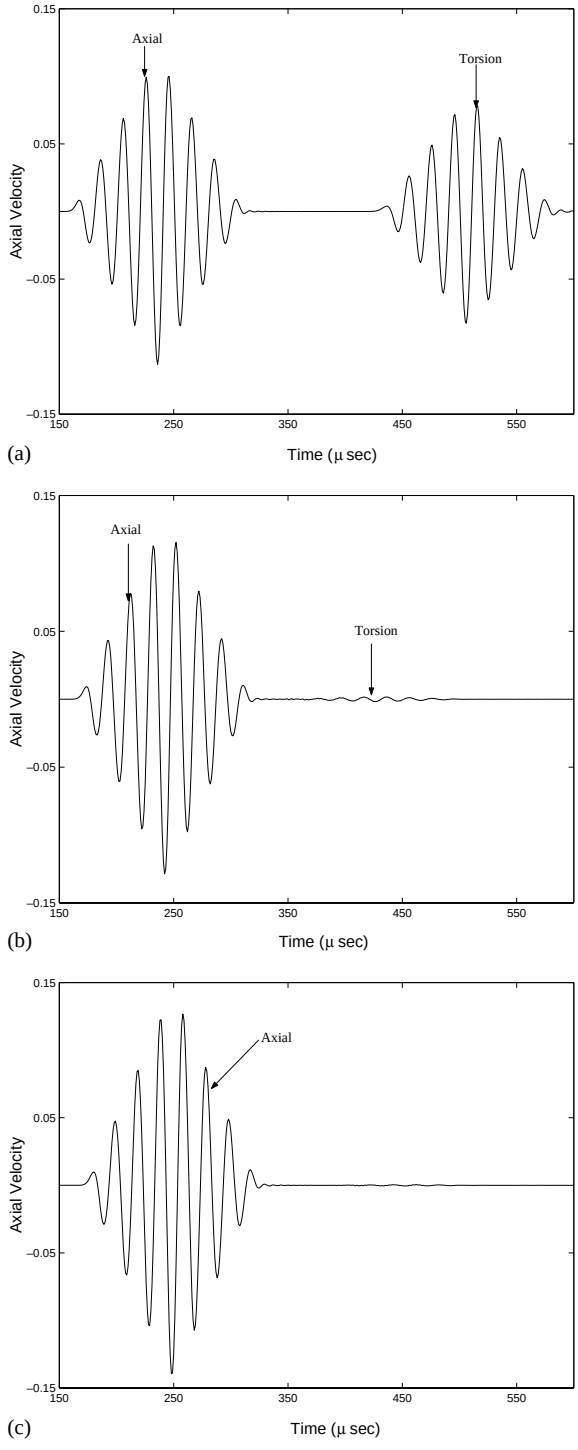

Fig. 16. Axial velocities of (a) $[15]_{AS}$, (b) $[30]_{AS}$, (c) $[45]_{AS}$ box-beam due to a sinusoidal pulse modulated at 50 kHz applied in axial direction. Torsion modes are shown in magnified scales.

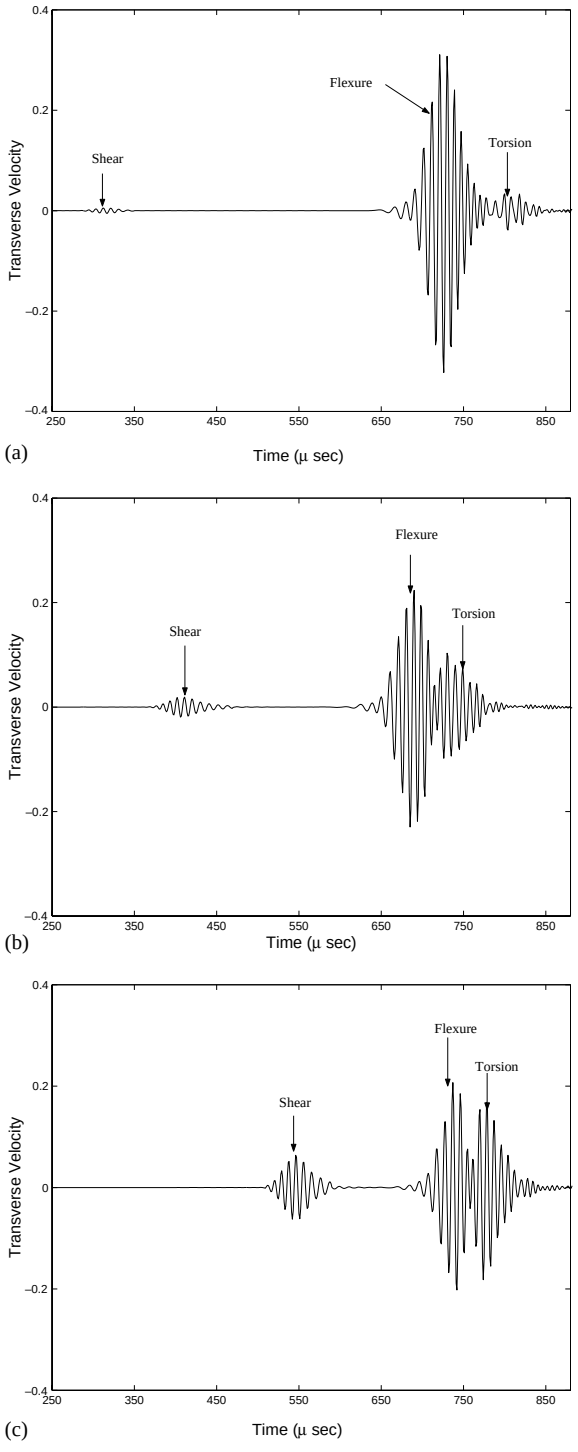

Fig. 17. Transverse velocities of (a) $[15]_S$, (b) $[30]_S$, (c) $[45]_S$ box-beam due to a sinusoidal pulse modulated at 110 kHz applied in transverse direction. Shear modes are shown in magnified scales.

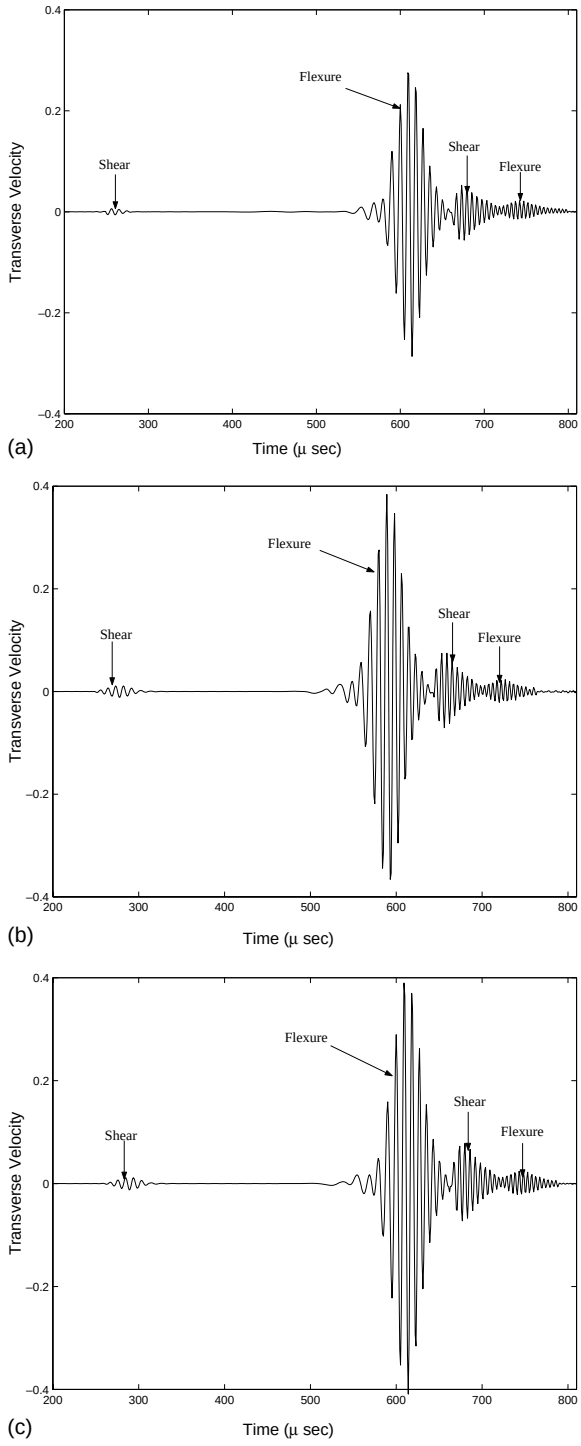

Fig. 18. Transverse velocities of (a) $[15]_{AS}$, (b) $[30]_{AS}$, (c) $[45]_{AS}$ box-beam due to a sinusoidal pulse modulated at 110 kHz applied in transverse direction. Shear modes and flexural mode in chordwise direction are shown in magnified scales.

on the infinite beam. The propagating length L is the distance between C and D. The beams of length 7.62 m are modeled with 5000 elements giving a system size of 6×5000. In all the cases responses are provided for beams with three ply orientation to show the effect of ply angle on the various coupling.

In a symmetric ply configuration $[\theta]_S$, the extension is coupled with shear in chordwise direction. Thus the axial velocity due to axial load will show two propagating modes. Fig. 15 shows the axial velocities for a modulated sinusoidal pulse with a modulated frequency of 50 kHz applied in axial direction. In the figure, the first blob is an axial mode, the second is the shear mode. The effect of shear coupling is more in $[30]_S$ and $[45]_S$ beam. Similarly an axial excitation to an antisymmetric ply configuration $[\theta]_{AS}$ gives extension torsion coupling. This is clearly seen in Fig. 16 for the same modulated sinusoidal pulse. The first blob is the axial mode while the second is the torsional mode. It is seen that extension–torsion coupling is strong only in $[15]_{AS}$ here. The propagating distance is $L = 0.5334$ m for both the above cases. In Figs. 17 and 18 the transverse velocities due to a sinusoidal pulse with a modulated frequency of 110 kHz applied in transverse direction is shown for symmetric and antisymmetric configurations respectively. The propagating lengths are $L = 1.2192$ m for $[\theta]_S$ and $L = 0.9144$ m for $[\theta]_{AS}$. $[\theta]_S$ ply orientations has a torsion, flexure and shear coupling and hence shows three propagating modes in Fig. 17. Similarly, four propagating modes can be visualized for $[\theta]_{AS}$ beam configuration having spanwise and chordwise shear and flexural coupling. From Fig. 17, we see the bending-torsion coupling is very high in $[45]_S$ while for $[15]_S$ it is less.

5. Conclusion

This paper present a generic thin walled composite beam element of arbitrary cross-section with open or closed contour. The refined element developed has super convergent property and is free from shear locking. The user does not have to know the situation where the shear deformation is predominant as the same element can be used for all situations. The formulation accounts for the non classical behaviors including elastic coupling, transverse shear and restrained torsional warping. Modeling of transverse shear deformation is based on FSDT and Vlasov theory is used for modeling of torsional warping. The element formulated is validated with various experimental, analytical and numerical results available both for static and dynamic cases. Various box beams and flat rectangular beam with different material properties and ply layup sequences are used as test cases. In all cases good correlation has been observed. Wave propagation analysis performed establish that effect of transverse shear is very pronounced at higher frequency ranges and produces a non-negligible decrease in wave velocities particularly in transverse direction. The various propagating coupling modes are graphically captured. The formulated beam element can be further refined by improving the cross-sectional stiffness modeling to get responses more comparable to 3-D finite element results. This refinement may help in more accurate high frequency or wave propagation analysis for various applications.

Appendix A

The non zero elements of the matrix $[A_1]$ and $[A_2]$ in Eq. (27) are given as

$$A_{1_{11}} = A_{11}, \quad A_{1_{12}} = A_{y_s16}, \quad A_{1_{14}} = A_{z_s16}, \quad A_{1_{16}} = A_{\alpha16}$$

$$A_{1_{17}} = -3A_{\varphi11}, \quad A_{1_{18}} = B_{11}, \quad A_{1_{19}} = \underline{B}_{11}$$

$$A_{1_{21}} = A_{y_s16}, \quad A_{1_{22}} = (A_{y_s^2 66} + A_{z_s^2 55}), \quad A_{1_{24}} = (A_{z_s y_s 66} - A_{z_s y_s 55}), \quad A_{1_{26}} = A_{y_s\alpha66}$$

$$A_{1_{27}} = -3A_{y_s\varphi16}, \quad A_{1_{28}} = B_{y_s16}, \quad A_{1_{29}} = \underline{B}_{y_s16}$$

$$A_{1_{33}} = 3(A_{y_s^2 66} + A_{z_s^2 55}), \quad A_{1_{35}} = 3(A_{z_s y_s 66} - A_{z_s y_s 55}), \quad A_{1_{37}} = 3A_{y_s \alpha 66}$$

$$A_{1_{38}} = (A_{z_s y_s 66} + A_{z_s z_n 55}), \quad A_{1_{39}} = (A_{y_s^2 66} + A_{z_s y_n 55})$$

$$A_{1_{41}} = A_{z_s 16}, \quad A_{1_{42}} = (A_{z_s y_s 66} - A_{z_s y_s 55}), \quad A_{1_{44}} = (A_{z_s^2 66} - A_{y_s^2 55})$$

$$A_{1_{46}} = A_{z_s \alpha 66}, \quad A_{1_{47}} = -3A_{z_s \varphi 16}, \quad A_{1_{48}} = B_{z_s 16}, \quad A_{1_{49}} = \underline{B}_{z_s 16}$$

$$A_{1_{53}} = 3(A_{z_s^2 66} + A_{y_s^2 55}), \quad A_{1_{55}} = 3A_{z_s \alpha 66}, \quad A_{1_{57}} = -3A_{\varphi 11}$$

$$A_{1_{58}} = (A_{z_s^2 66} - A_{z_n y_s 55}), \quad A_{1_{59}} = (A_{z_s y_s 66} - A_{y_n y_s 55})$$

$$A_{1_{61}} = A_{\alpha 16}, \quad A_{1_{62}} = A_{y_s \alpha 66}, \quad A_{1_{63}} = 3A_{y_s \varphi 16}, \quad A_{1_{64}} = A_{z_s \alpha 66}$$

$$A_{1_{65}} = 3A_{z_s \varphi 16}, \quad A_{1_{66}} = A_{\alpha^2 66}, \quad A_{1_{68}} = (B_{\alpha 16} + A_{z_s \varphi 16}), \quad A_{1_{69}} = (\underline{B}_{\alpha 16} + A_{y_s \varphi 16})$$

$$A_{1_{73}} = 3A_{y_s \alpha 66}, \quad A_{1_{75}} = 3A_{z_s \alpha 66}, \quad A_{1_{77}} = 3A_{\alpha^2 66}, \quad A_{1_{78}} = A_{z_s \alpha 66}, \quad A_{1_{79}} = A_{y_s \alpha 66}$$

$$A_{1_{81}} = B_{11}, \quad A_{1_{82}} = B_{y_s 16}, \quad A_{1_{84}} = B_{z_s 16}, \quad A_{1_{86}} = (A_{z_s \varphi 16} + B_{\alpha 16})$$

$$A_{1_{87}} = -3B_{\varphi 11}, \quad A_{1_{88}} = D_{11}, \quad A_{1_{89}} = \widetilde{D}_{11}$$

$$A_{1_{91}} = \underline{B}_{11}, \quad A_{1_{92}} = \underline{B}_{y_s 16}, \quad A_{1_{94}} = \underline{B}_{z_s 16}, \quad A_{1_{96}} = (A_{y_s \varphi 16} + \underline{B}_{\alpha 16})$$

$$A_{1_{97}} = -3\underline{B}_{\varphi 11}, \quad A_{1_{98}} = \widetilde{D}_{11}, \quad A_{1_{99}} = \underline{D}_{11}$$

All other $A_{1_{ij}} = 0$.

$$A_{2_{19}} = -0.5A_{z_s 16}, \quad A_{2_{111}} = -0.5A_{y_s 16}$$

$$A_{2_{210}} = -0.5(A_{z_s y_s 66} + A_{z_s z_n 55}), \quad A_{2_{212}} = -0.5(A_{y_s^2 66} + A_{z_s y_n 55})$$

$$A_{2_{410}} = -0.5(A_{z_s^2 66} - A_{z_n y_s 55}), \quad A_{2_{412}} = -0.5(A_{z_s y_s 66} - A_{y_s z_n 55})$$

$$A_{2_{610}} = -0.5A_{z_s \alpha 66}, \quad A_{2_{612}} = -0.5A_{y_s \alpha 66}$$

$$A_{2_{82}} = 0.5A_{z_s 16}, \quad A_{2_{84}} = 0.5(A_{z_s y_s 66} + A_{z_s z_n 55}), \quad A_{2_{86}} = 0.5(A_{z_s^2 66} + A_{z_n y_s 55})$$

$$A_{2_{88}} = 0.5A_{z_s \alpha 66}$$

$$A_{2_{89}} = 0.5(A_{z_s^2 66} + A_{z_n^2 55}), \quad A_{2_{811}} = 0.5(A_{z_s y_s 66} + A_{z_n y_s 55}), \quad A_{2_{812}} = -0.5(B_{y_s 16} - \underline{B}_{z_s 16})$$

$$A_{2_{92}} = 0.5A_{y_s 16}, \quad A_{2_{94}} = 0.5(A_{y_s^2 66} + A_{z_s y_n 55}), \quad A_{2_{96}} = 0.5(A_{z_s^2 66} - A_{y_s y_n 55})$$

$$A_{2_{98}} = 0.5A_{y_s \alpha 66}$$

$$A_{2_{99}} = 0.5(A_{z_s y_s 66} + A_{z_n y_n 55}), \quad A_{2_{910}} = 0.5(B_{y_s 16} - \underline{B}_{z_s 16}), \quad A_{2_{911}} = 0.5(A_{z_s y_s 66} + A_{y_n^2 55})$$

All other $A_{2_{ij}} = 0$.

References

Abarcar, R.B., Cuniff, P.F., 1972. The vibration of cantilever beams of fiber reinforced material. Journal of Composite Materials 10 (6), 504–517.

Averill, R.C., Reddy, J.N., 1990. On the behavior of plate elements based on the first order theory. Engineering Computation 7, 57–74.

Badir, A.M., Berdichevsky, V.L., Armanios, E.A., 1993. Theory of Composite Thin Walled Opened Cross-Section Beams. In: Proceedings of AIAA/ASME/ASCE/AHS/ASC 34th Structures, Structural Dynamics and Materials Conference, pp. 2761–2770.

Bazoune, A., Khulief, Y.A., Stephen, N.G., 2003. Shape functions of three-dimensional timoshenko beam element. Journal of Sound and Vibration 259, 473–480.

Berdichevsky, V.L., Armanios, E., Badir, A., 1992. Theory of anisotropic thin walled closed cross-section beams. Composites Engineering 2 (5–7), 411–432.

Cesnik, C.E.S., Hodges, D.H., 1997. VABS: a new concept for composite rotor blade cross-sectional modeling. Journal of American Helicopter Society 42 (1), 27–38.

Chakraborty, A., Mahapatra, D.R., Gopalakrishnan, S., 2001. Finite element analysis of free vibration and wave propagation in antisymmetric beams with structural discontinuities. Composite Structures 55 (1), 23–36.

Chandra, R., Chopra, I., 1991. Experimental and theoretical analysis of composite I-beams with elastic couplings. AIAA Journal 29 (12), 2197–2203.

Chandra, R., Chopra, I., 1992. Experimental and theoretical investigation of the vibration characteristics of rotating composite box beams. Journal of Aircraft 29 (4), 657–664.

Chandra, R., Stemple, A.D., Chopra, I., 1990. Thin walled composite beams under bending, torsional and extensional loads. Journal of Aircraft 27 (7), 619–626.

Davalos, J.F., Kim, Y., Barbero, E.J., 1994. Analysis of laminated beams with a layer-wise constant shear theory. Composite Structure 28, 241–253.

Eisenberger, M., 1994. Derivation of shape functions for an exact 4 d.o.f. timoshenko beam element. Communications in Numerical Methods in Engineering 10, 673–681.

Eisenberger, M., 2003. An exact high order beam element. Computers and Structures 81, 147–152.

Friedman, Z., Kosmatka, J.B., 1993. An improved two node timoshenko beam finite element. Composite Structures 47, 473–481.

Gopalakrishnan, S., 2000. A deep rod finite element for structural dynamics and wave propagation problems. International Journal for Numerical Methods in Engineering 48, 731–744.

Gopalakrishnan, S., Martin, M., Doyle, J., 1992. A matrix methodology for spectral analysis of wave propagation in multiple connected timoshenko beam. Journal of Sound and Vibration 158 (1), 11–24.

Hodges, D.H., Atilgan, A.R., Fulton, M.V., Rehfield, L.W., 1991. Free vibration analysis of composite beams. Journal of American Helicopter Society 36 (3), 36–47.

Jones, R.M., 1975. Mechanics of Composite Materials. McGraw-Hill, New York.

Jung, S.N., Nagaraj, V.T., Chopra, I., 1999a. A General Structural Model for Thin and Thick Walled Composite Blades with Elastic Coupling. 24th European Rotorcraft Forum, Marseilles, France.

Jung, S.N., Nagaraj, V.T., Chopra, I., 1999b. Assessment of composite rotor blade modeling techniques. Journal of American Helicopter Society 44 (3), 188–205.

Jung, S.N., Nagaraj, V.T., Chopra, I., 2001. Refined structural dynamics model for composite rotor blades. AIAA Journal 39 (2), 339–348.

Jung, S.N., Nagaraj, V.T., Chopra, I., 2002. Refined structural model for thin and thick walled composite rotor blades. AIAA Journal 40 (1), 105–116.

Kant, T., Gupta, A., 1988. A finite element model for a higher order shear deformable beam theory. Journal of Sound and Vibration 125 (2), 193–202.

Khedir, A.A., Reddy, J.N., 1997. An exact solution for the bending of thin and thick cross ply beam. Composite Structures 37, 195–203.

Lin, X., Yuan, F.G., 2001. Diagnostic lamb waves in an integrated piezoelectric sensor/actuator plate: analytical and experimental studies. Smart Materials and Structures 10, 907–913.

Mahapatra, D.R., Gopalakrishnan, S., Sankar, T.S., 2000. Spectral-element based solution for wave propagation analysis of multiply connected unsymmetrical laminated composite beams. Journal of Sound and Vibration 237 (5), 819–836.

Megson, T.H.G., 1974. Linear Analysis of Thin-Walled Elastic Structures. Surrey University Press.

Nag, A., Mahapatra, D.R., Gopalakrishnan, S., 2002. Identification of delamination in a composite beam using a damaged spectral element. Structural Health Monitoring 1 (1), 105–126.

Popescu, B., Hodges, D.H., 1999. On asymptotically correct Timoshenko-like anisotropic beam theory. International Journal of Solids and Structures 37 (3), 535–558.

Reddy, J.N., 1997. On locking free shear deformable beam finite elements. Computer Methods in Applied Mechanics and Engineering 149, 113–132.

Smith, E.C., Chopra, I., 1991. Formulation and evaluation of an analytical model for composite box-beams. Journal of American Helicopter Society 36 (3), 23–35.

Song, O., Librescu, L., 1997. Structural modeling and free vibration analysis of rotating composite thin-walled beams. Journal of American Helicopter Society 42 (4), 358–369.

Stemple, A.D., Lee, S.W., 1989. Large deflection static and dynamic analyses of composite beams with arbitrary cross-sectional warping. In: Proceedings of the AIAA/ASME/ASCE/AHS/ASC 30th Structures, Structural Dynamics, and Materials Conference. AIAA, Washington, DC, pp. 1788–1798.

Suresh, J.K., Nagaraj, V.T., 1996. Higher order shear deformation theory of thin walled composite beams. Journal of Aircraft 33 (5), 978–986.

Valdés, S.H.D., Soutis, C., 2001. A structural health monitoring system for laminated composites. In: Proceedings of ASME Design Engineering Technical Conference, Pittsburgh, Pennsylvania, USA.

Volovoi, V.V., Hodges, D.H., 2002. Single and multicelled composite thin walled beams. AIAA Journal 40 (5), 960–965.

Volovoi, V.V., Hodges, D.H., Cesnik, C.E.S., Popescu, B., 2001. Assessment of beam modeling methods for rotor blade applications. Mathematical and Computer Modelling 33 (10–11), 1099–1112.

Yu, W., Volovoi, V.V., Hodges, D.H., Hong, X., 2002. Validation of the variational asymptotic beam sectional analysis. AIAA Journal 40 (10), 2105–2112.